Journal of Solid State Electrochemistry (2018) 22:2767–2774
https://doi.org/10.1007/s10008-018-3962-7

ORIGINAL PAPER

Facile synthesis of $CoWO_4$/RGO composites as superior anode materials for lithium-ion batteries

Feihui Li[1,2] · HeYa Na[3] · Wei Jin[4] · Xiaoyang Xu[3] · Wei Wang[5] · Jianping Gao[3]

Received: 1 November 2017 / Revised: 29 March 2018 / Accepted: 7 April 2018 / Published online: 11 May 2018

Abstract

In this paper, a facile method has been developed to synthesize supported $CoWO_4$ on the reduced graphene oxide (RGO) as high-performance anode material for Li-ion batteries. The composites with cuboid-like $CoWO_4$ nanoparticles were prepared by directly adding graphene oxide into the precursor solution followed by a hydrothermal treatment. Different analytical methods like high-resolution TEM, XRD, TGA, and XPS characterizations were employed to illustrate structural information of the as-prepared $CoWO_4$ and $CoWO_4$/RGO composites. In addition, the Li-ion battery performance using the composites as anode materials was also discussed based on the detailed galvanostatic charge-discharge cycling tests. The result shows that the specific capacity of the as-prepared $CoWO_4$/RGO composites can reach 533.3 mAh g^{-1} after 50 cycles at a current density of 100 mA g^{-1}. During the whole cyclic process, the coulombic efficiency was maintained higher than 90%. Therefore, $CoWO_4$, as an environment-friendly and cost-effective anode material, has promising potential for Li-ion batteries.

Keywords $CoWO_4$ nanocubes · RGO · Composite · Li-ion battery · Anode

Introduction

Lithium-ion batteries (LIBs) have been successfully employed in lots of portable electronic devices owing to their superior properties of high energy density, excellent rate capability, long cycle life, and environmental friendliness [1–3]. In recent years, carbon-based anode materials for lithium-ion batteries are widely used in commercial field, but they cannot meet the growing demand of high-energy applications due to their low theoretical capacity (372 A h/g) and security [4]. Hence, in order to improve the performance of LIBs, it is highly desirable to develop high-performance anode materials with high capability.

Since Poizot et al. discovered that transition metal oxides exhibit high capacities as anode materials [5], novel metal oxides, and composite oxides have been extensively studied as promising alternative to carbon-based anode materials in Li-ion batteries. The high electrochemical performance is attributed to their low lithium insertion potential and high volumetric and gravimetric capacities [6], e.g., Fe_2O_3, Fe_3O_4, CoO, Co_3O_4, and CuO [2, 7–10]. Besides, the mechanism of Li reactivity in these systems differs from the classical Li insertion/de-insertion or Li-alloying processes; it involves the reduction and oxidation of metal nanoparticles.

Tungsten is a high-performance metal due to its robust and high melting point nature, and it has been demonstrated that tungsten-containing metal oxides have potential applications in many areas [1]. As a member of these materials, tungstate is a kind of active material that has been applied in electrochemical devices, including anode materials of LIBs [4, 11–14]. Besides, the binary metal oxide $CoWO_4$, one of the tungstates, has attracted increasing attentions for its multitude of applications, including catalysts for oxygen evolution [15] and

✉ Feihui Li
tjlifeihui@126.com

✉ Jianping Gao
jianpingg@eyou.com

[1] Department of Applied Chemistry, College of Biotechnology and Food Science, Tianjin University of Commerce, Tianjin 300134, People's Republic of China

[2] Sichuan Province Metal Fuel Cell Key Laboratory, Deyang 618000, Sichuan, People's Republic of China

[3] School of Science, Tianjin University, Tianjin 300072, People's Republic of China

[4] Institute of Process Engineering, Chinese Academy of Sciences, Beijing 100190, People's Republic of China

[5] School of Chemical Engineering and Technology, Tianjin University, Tianjin 300072, People's Republic of China

hydrogen production [16]. Yu et al. have used $CoWO_4$ nanoparticles wrapped by reduced graphene oxide (RGO) as anode material for lithium-ion batteries [17]. They synthesized three samples $CoWO_4$-RGO_1, $CoWO_4$-RGO, and $CoWO_4$-RGO_1, and their $CoWO_4$ contents are 5, 10.8, and 26.6%, respectively. Of the three samples, $CoWO_4$-RGO delivers the best electrochemical performance when they are used as the anodes of the LIB. It is worth noticeable that the anode material $CoWO_4$-RGO is mainly composed of RGO (89.2%).

However, there are two bottleneck problems for the application of tungstate material as anodes in lithium-ion batteries: the high initial irreversible capacity and poor electronic conduction during the alloying and de-alloying process, which lead to poor cycling performance [4]. Consequently, considerable efforts have been devoted to overcome these problems. In comparison with pure metal oxide, incorporating with second metal can greatly enhance the conductivity of binary metal oxides [18]. In addition, adding graphene sheets into materials is another way to significantly improve the electrochemical performance of transition metal oxide composites [19–24]. In these graphene-contained composites, the cycling stability and rate capability of transition metal oxide anodes are enhanced due to the increased electrical conductivity and anode/electrolyte contact area [25–27].

In this paper, we report a hydrothermal method for facile synthesis of $CoWO_4$ nanocubes/reduced graphene oxide ($CoWO_4$/RGO) composites as anode materials for LIB application. The $CoWO_4$/RGO composites contain mainly $CoWO_4$, so they are different from the abovementioned $CoWO_4$-RGO, in which RGO is the main component [17]. In addition, the preparation conditions of the present work are also different from the $CoWO_4$-RGO. The $CoWO_4$/RGO composites combine the advantages of $CoWO_4$ nanocubes and graphene, in which the graphene sheets can improve the electrical conductivity and structural stability of the $CoWO_4$ nanocubes. As an anode of LIB, the $CoWO_4$/RGO composite exhibits a stable capacity of ~ 533 mAh g^{-1} after 50 cycles at a current density of 100 mA g^{-1}. Moreover, it retains a capacity of ~ 440 mAh g^{-1} even at a high current density of 500 mA g^{-1}, demonstrating its potential applications for LIBs with long cycling life and high power density.

Experimental

Materials

Natural graphite powder was purchased from the Qingdao Graphite Factory. Potassium permanganate, sodium nitrate, concentrated sulfuric acid, hydrogen peroxide (30%), hydrochloric acid, cobalt chloride ($CoCl_2$), and sodium tungstate (Na_2WO_4) were from Sigma, and all the unmentioned reagents were purchased from the Tianjin Chemical Reagent Company. All the chemicals were used as received without additional purification.

Synthesis of $CoWO_4$ and $CoWO_4$/RGO composites

In a typical process, 25 mL $CoCl_2$ aqueous solution (0.1 mol L^{-1}) was added into 25 mL Na_2WO_4 aqueous solution (0.1 mol L^{-1}) with the assistance of strong magnetic stirring to form a homogeneous precursor at room temperature. After being stirred for another 10 min, the final mixture was directly transferred into a 100-mL Teflon-lined stainless autoclave, filled up to 50% of its capacity. The autoclave was maintained at 160 °C for 24 h in an oven and then was cooled naturally to the room temperature. The precipitate was collected, filtered, and washed with distilled water and absolute ethanol several times. After being dried at 50 °C for 2 h, the $CoWO_4$ powders were obtained [28].

A modified Hummers' method was employed to produce graphite oxide from natural graphite powder. The graphene oxide suspension for $CoWO_4$/RGO synthesis was prepared by ultrasonicating graphite oxide in distilled water. To synthesize $CoWO_4$/RGO via a typical process, 25 mL $CoCl_2$ aqueous solution (0.1 mol L^{-1}) was added into 25 mL Na_2WO_4 aqueous solution (0.1 mol L^{-1}) with the assistance of strong magnetic stirring to form a homogeneous precursor at room temperature. The solution was then added to 6 mL graphene oxide suspension (5 mg mL^{-1}) with stirring. After stirring for 20 min, the final mixture was directly transferred into a 100-mL Teflon-lined stainless autoclave to fill up to 56% of its capacity. The autoclave was maintained at 160 °C for 24 h in an oven and then cooled naturally to the room temperature. The precipitate was collected, filtered, and washed with distilled water and absolute ethanol several times. After being dried at 50 °C for 2 h, the obtained powder is noted as

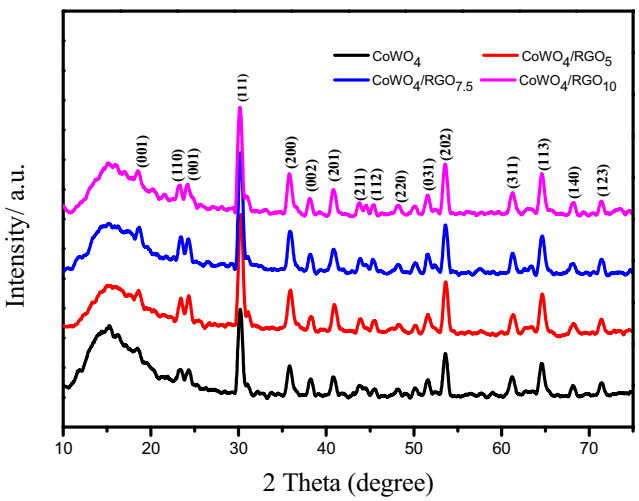

Fig. 1 XRD patterns of $CoWO_4$ and $CoWO_4$/RGO composites

$CoWO_4/RGO_5$ ($CoWO_4/RGO_5$ means that GO content is 5% wt). The $CoWO_4$/RGO composites with other content were also prepared by adding different amount of GO.

Characterization of $CoWO_4$/RGO nanocomposites

The structure and morphology of the $CoWO_4$/RGO composites were characterized by the transmission electron microscope (Philips Tecnai G^2F20 microscope). X-ray diffraction (XRD) of the $CoWO_4$/RGO composites was measured using an X-ray diffractometer (BDX3300) with a reference target: Cu Ka radiation ($\lambda = 1.54$ Å), voltage 30 kV, and current 30 mA. Thermal gravimetric analysis (TGA) of the $CoWO_4$/RGO was conducted on a Rigaku-TD-TDA analyzer with a heating rate of 10 °C/min in air. Elemental analysis of the $CoWO_4$/RGO composites was determined by an X-ray photoelectron spectrometer with a Mg Ka anode (PHI1600 ESCA System, PERKIN ELMER, USA).

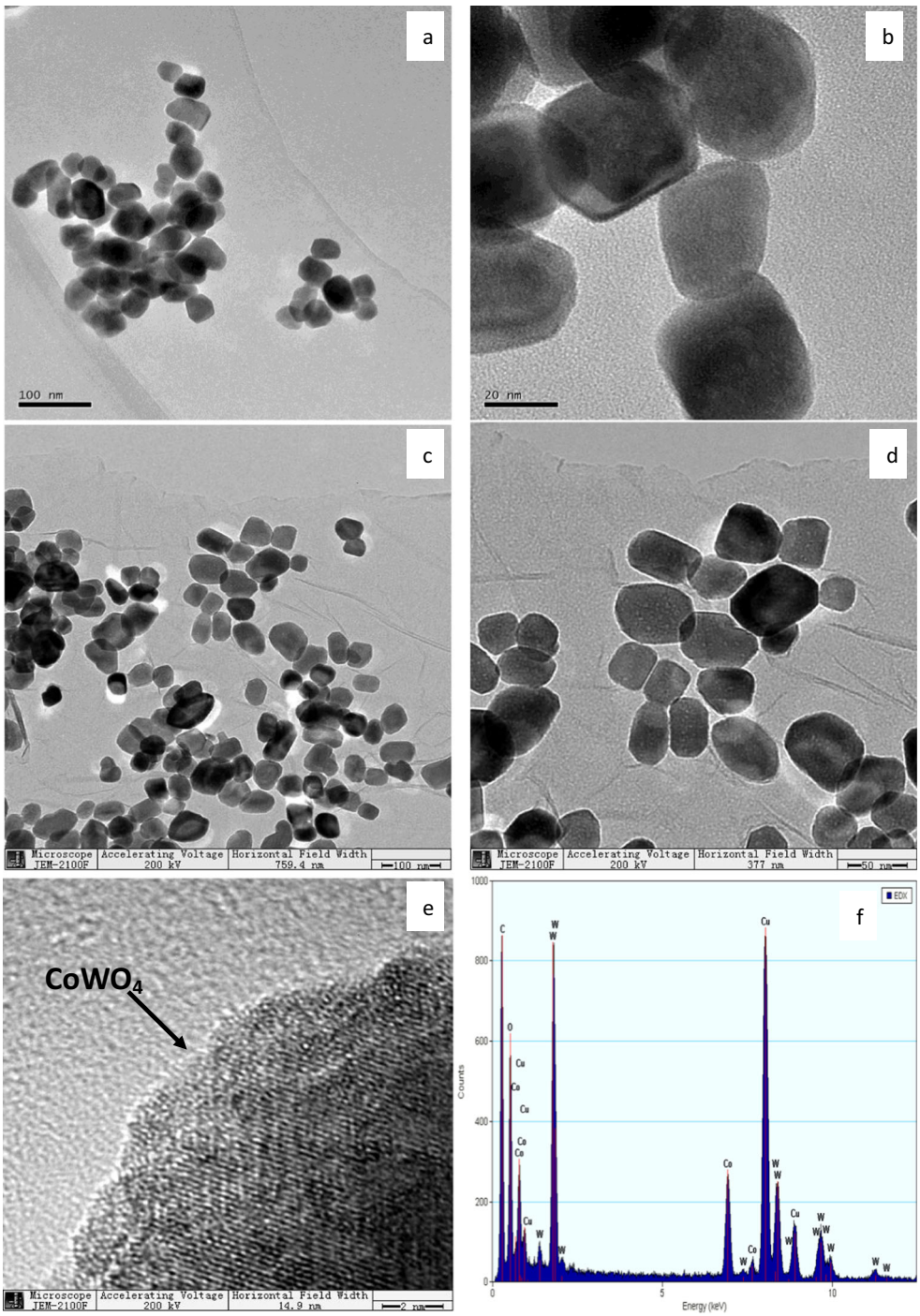

Fig. 2 TEM images of $CoWO_4$ (**a**, **b**) and $CoWO_4/RGO_5$ (**c**, **d**). HRTEM images of $CoWO_4$/RGO_5 (**e**) and the EDX spectrum of $CoWO_4/RGO_5$ (**f**)

Electrochemical measurements

Active materials ($CoWO_4$/RGO, $CoWO_4$, or RGO), carbon black (as conductive agent), and polyvinylidene fluoride (PVDF as a binder) in a weight ratio of 80:10:10 were mixed with *N*-methylpyrrolidone (NMP) to form a slurry. The slurry was then dropped on a piece of copper foam and treated in a vacuum oven at 50 °C for 12 h. The copper foam was dried before it was pressed to form a disk. Coin cells (CR2032) were assembled with the disk as an anode, lithium metal as a counter electrode, Celgard 2400 as separator, and $LiPF_6$ (1 M) in ethylene carbonate/dimethyl carbonate/diethyl carbonate (EC/DMC/DEC, 1:1:1 vol%) as an electrolyte. The cells were assembled in a glove box filled with Ar gas. The rate capability and cycle life of the cells were tested in a potential window of 0.01~3 V (vs Li^+/Li) with a battery testing system (LAND CT 2001A).

Results and discussion

$CoWO_4$/RGO and $CoWO_4$ were synthesized by a facile hydrothermal approach. In order to identify the products, XRD analysis was performed and the XRD patterns of the as-prepared $CoWO_4$ and $CoWO_4$/RGO with different initiate GO amount ($CoWO_4$/RGO_5 means that GO is 5% wt) are shown in Fig. 1. Obviously, $CoWO_4$ and all the $CoWO_4$/RGO composites have similar XRD patterns that match with monoclinic $CoWO_4$ with wolframite structure (JCPDS: 15-0867) [29]. Their strongest intensity peaks are all located at 30.68° diffracted from (-111) planes of the $CoWO_4$ [29]. Since no other characteristic peaks of impurities were detected, we can get the conclusion that the products are pure $CoWO_4$ or $CoWO_4$/RGO composites.

Figure 2 presents TEM micrographs of $CoWO_4$ (Fig. 2a, b) and $CoWO_4$/RGO_5 (Fig. 2c, d), respectively. It is clear that the as-prepared $CoWO_4$ and $CoWO_4$/RGO_5 are composed of nano-sized $CoWO_4$ particles with homogeneous cuboid-like morphology and $CoWO_4$/RGO_5 (Fig. 2c, d) also shows the wrinkles on RGO nanosheets. Figure 2e is a HRTEM image of an individual $CoWO_4$ nanoparticle; the clear lattice fringes further confirm its crystalline nature as demonstrated by XRD analysis. Energy dispersive X-ray spectrum (EDS) (Fig. 2f) shows only high-intensity peaks for Co, W, and O, together with the Cu and C (partly from rGO) peaks generated from a carbon film-supported copper grid. Quantitative

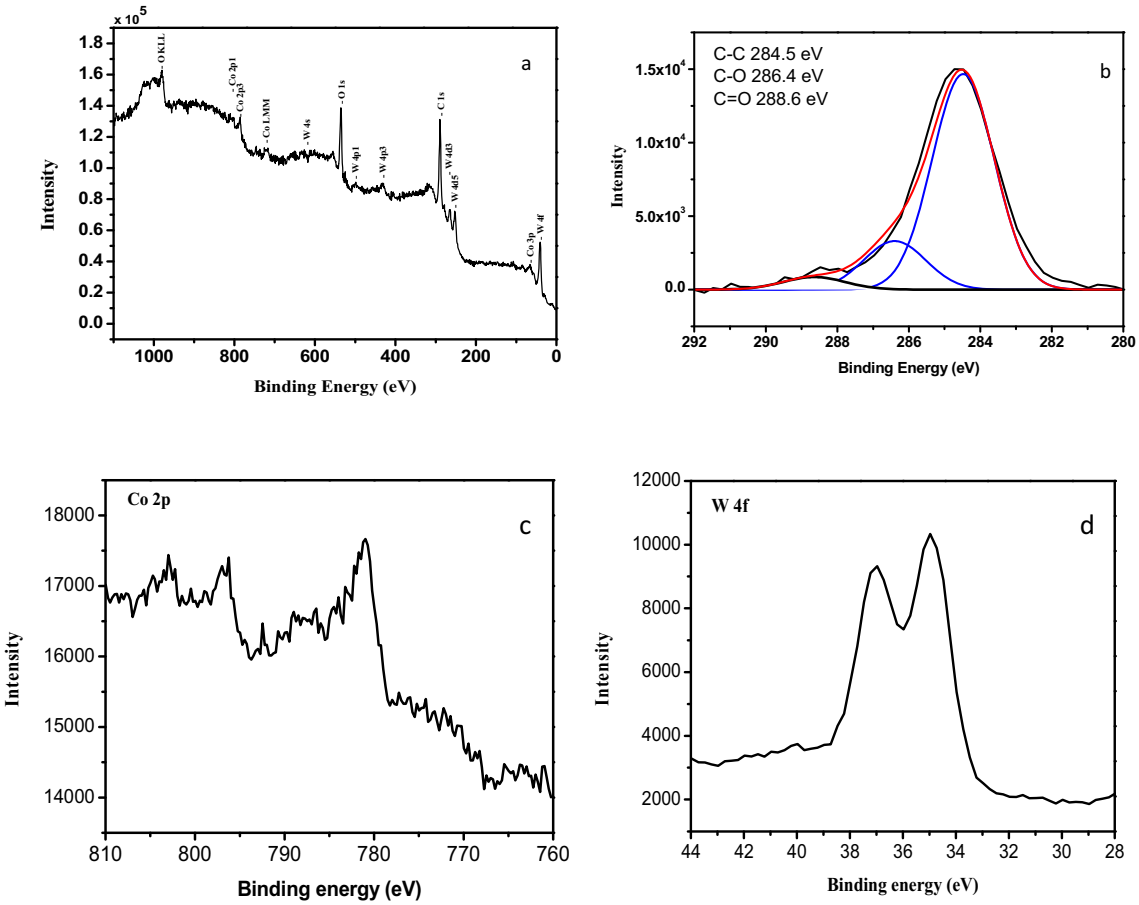

Fig. 3 XPS spectrum of $CoWO_4$/RGO_5 (**a**) and XPS spectra for C1s (**b**), Co 2P (**c**), and W 4f (**d**) in $CoWO_4$/RGO_5

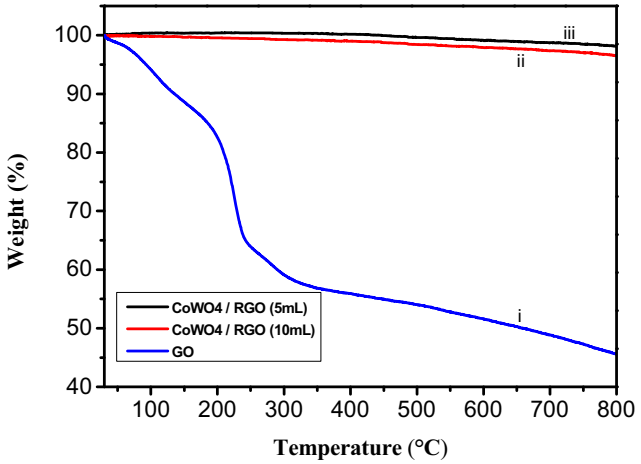

Fig. 4 TGA curves of GO (i), $CoWO_4/RGO_{10}$ (ii), and $CoWO_4/RGO_5$ (iii)

calculation shows that the molar ratio of Co to W is about 1:1, which is in agreement with the nominal composition of $CoWO_4$.

Figure 3a presents the X-ray photoelectron spectroscopy (XPS) spectrum of $CoWO_4/RGO_5$ composites in order to confirm surface composition and energy state structure of the sample. The spectrum contains four strong peaks: a C1s peak at about 286 eV, an O1s peak at about 532 eV, a Co 2p peak at about 792 eV, and a W 4f peak at about 35 eV. The O peaks stem from both $CoWO_4$ and RGO, C peaks come from RGO and Co, and W peak comes from $CoWO_4$. The high-resolution XPS of C1s, Co 2p, and W 4f are shown in Fig. 3b–d, respectively. The C1s XPS spectrum of $CoWO_4/RGO_5$ (Fig. 3b) demonstrates three different groups of bands, a sp2-bonded carbon network (C–C/C=C, 284 eV), hydroxyl and epoxy groups (C–O, 286 eV), and carbonyl groups (C=O, 288 eV) [30]. The C/O ratio of RGO in $CoWO_4$/RGO is 4.65, which is higher than that of GO (2.30). This indicates that after the hydrothermal process, many oxygen-containing functional groups were removed away, suggesting that GO was successfully reduced [31]. The Co 2p electron peaks and two satellite peaks well match with the previous report [32]. The spectrum of the W 4f exhibits a main peak at 35.15 eV as well as a peak at 37.20 eV, which belongs to a simple spin-doublet W 4f7/2 and W 5p3, respectively [33]. This indicates that the oxidation state of tungsten is + 6. The above XPS results further prove the formation of $CoWO_4/RGO_5$ composites.

TGA analysis was conducted on GO (Fig. 4, curve i), $CoWO_4/RGO_5$ (Fig. 4, curve iii), and $CoWO_4/RGO_{10}$ (Fig. 4, curve ii). For GO, a weight loss of about 30% occurred between 100 and 200 °C. This is due to the removal of the surface water and the oxygen-containing functional groups (such as C–O and C=O) [34]. At the temperature above 200 °C, the weight loss may be due to the removal of the remaining oxygen-containing functional groups [31]. It is clear that the total weight loss of $CoWO_4/RGO_5$ and $CoWO_4/RGO_{10}$ is much smaller than GO. It indicates that the GO has been reduced during the hydrothermal treatment, which is in accordance with the XPS results.

The electrochemical performance of the prepared $CoWO_4$ and $CoWO_4/RGO_5$ composites for Li-ion anodic materials was investigated. Figure 5a shows the cyclic voltammetric (CV) curves at a scan rate of 0.5 mV s^{-1} in the potential range from 0.01 to 3.00 V at room temperature [35]. Two reduction peaks are observed in the cathodic scan. The peaks at around 1.5 and 0.5 V are ascribed to the reduction of Co^{2+} and W^{6+} to Co and W [36, 37]. The corresponding anodic peaks represent the oxidation reactions, in which Li_2O is activated to release Li^+ by Co and W. Figure 5b shows the galvanostatic charge-discharge (GCD) curves of the $CoWO_4/RGO_5$ for the first three cycles at a current density of 100 mA g^{-1}. In the potential range from 0.01 to 3 V, it is noted that the first discharge

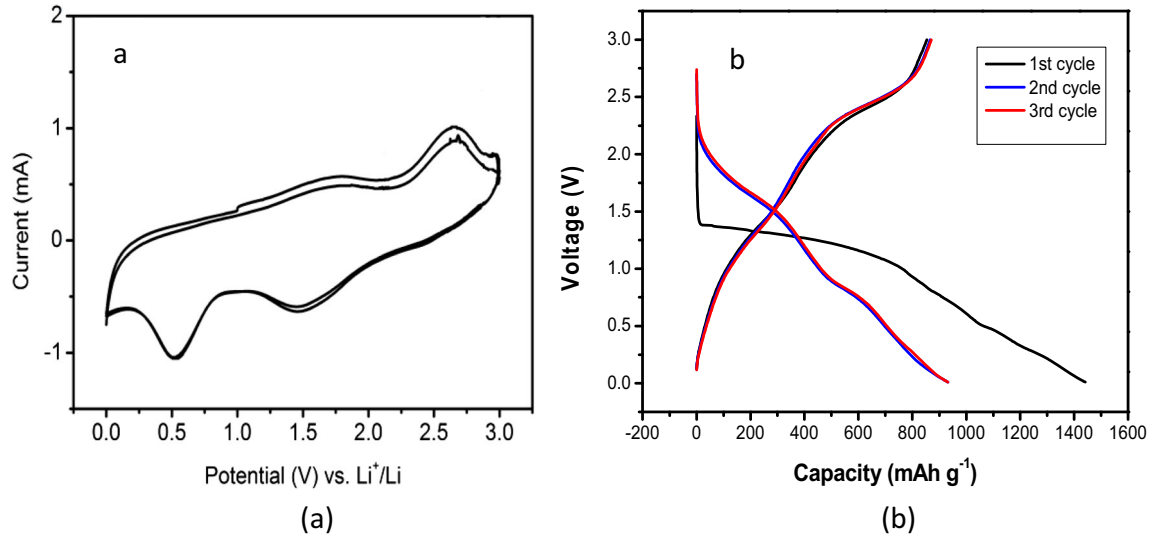

Fig. 5 Cycling performance (**a**) and galvanostatic charge-discharge curves (**b**) of the $CoWO_4/RGO_5$ electrodes

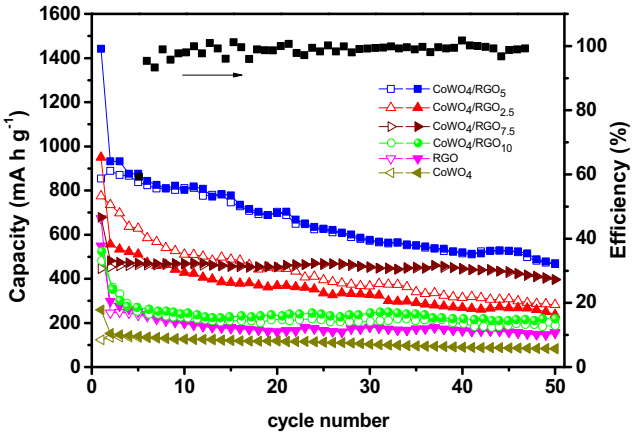

Fig. 6 Cycling performances of $CoWO_4$/RGO composites, $CoWO_4$, and RGO anodes charged and discharged at a current of 100 mA g^{-1} up to 100 cycles

profile has a plateau region at about 1.5 V which corresponds to the reduction reaction of the $CoWO_4$/RGO_5 and the result could be confirmed by the above CV analysis. From the second cycle, the discharge profiles indicate relatively constant lithiation and delithiation processes. The discharge/charge process can be illustrated as follows based on the above discussion [37, 38]:

$$CoWO_4 + 8\,Li^+ + 8\,e^- \rightarrow Co + W + 4\,Li_2O \quad (1)$$

$$Co + Li^+ + e^- \rightleftarrows LiZn \quad (2)$$

$$LiCo + W + 3\,Li_2O \rightleftarrows Zn + WO_3 + 6\,Li^+ + 6\,e^- \quad (3)$$

Figure 6 compares the cycling performances of different electrodes at a current of 100 mA g^{-1} during 50 cycles: $CoWO_4$, RGO, and different $CoWO_4$/RGO composites. Significantly, the $CoWO_4$/RGO electrode exhibited a much higher cycling capacity than the $CoWO_4$ and RGO electrodes. For example, the $CoWO_4$/RGO_5 electrode reached a high capacity of 810 mAh g^{-1} after 10 cycles while only 122 mAh g^{-1} for $CoWO_4$ electrode and 208 mAh g^{-1} for RGO electrode were obtained, respectively. After 50 cycles, the $CoWO_4$/RGO_5 electrode remained 533 mAh g^{-1} while the $CoWO_4$ and RGO electrodes retained about 75 and 157 mAh g^{-1}, respectively. On the other hand, the coulombic efficiency of the $CoWO_4$/RGO_5 electrode was almost 95% during the 50 cycles. These results imply available lithium insertion-extraction and efficient ion and electron transport within the electrodes. The enhanced electrochemical performance of the $CoWO_4$/RGO composites can be attributed to the synergistic effect between RGO and $CoWO_4$, which could enhance the electrical conductivity, facile the contact electrode and electrolyte, shorten the transport pathway for both electrons and ions, and depress volume expansion during the prolonged cycling [22, 39–41]. For composite materials, there is generally an optimal composition at which the composite displays the best performance [42].

Rate performance is a vital measurement to evaluate the potential practical application of the anode electrode [43, 44]. The results in Fig. 7 also show that the $CoWO_4$/RGO_5 composite has a high rate capability. As shown in Fig. 7a, the $CoWO_4$/RGO_5 composite demonstrated much higher capacities of 980, 660, 384, 217, and 188 mAh g^{-1} after each 10 cycles at 0.1, 0.2, 0.5, 1, and 1.1 A g^{-1} than those of $CoWO_4$ (238, 140, 78, 44, and 43 mAh g^{-1} at 0.1, 0.2, 0.5, 1, and 1.1 A g^{-1} shown in Fig. 7b), suggesting that the RGO in the composite plays a key role for enhancing rate performance. In addition, a capacity of 545 mAh g^{-1} was still recovered when the current rate was returned to 100 mA g^{-1}. These results reveal that the $CoWO_4$/RGO_5 composite electrode has better electrochemical reversibility and structural stability than the pure $CoWO_4$ electrode.

In order to gain insight into the remarkable rate performance of the electrodes, EIS measurements were carried out.

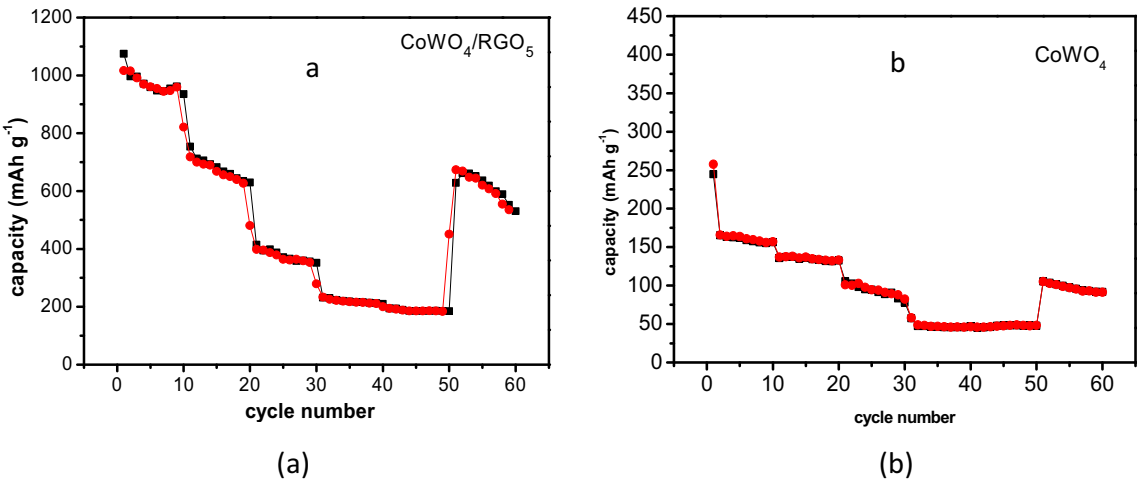

Fig. 7 Rate performance of the $CoWO_4$/RGO_5 (**a**) and $CoWO_4$ (**b**) electrodes

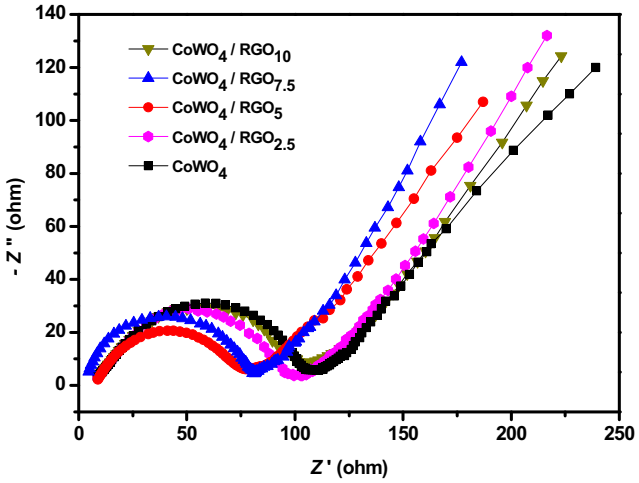

Fig. 8 Nyquist plots of $CoWO_4$/RGO composites and $CoWO_4$ electrodes

All the Nyquist plots in Fig. 8 display a typical pattern, a semicircle and a sloping straight line in the high and low frequency range, respectively. The diameter of the semicircle reflects the charge-transfer resistance at the electrode/electrolyte interfaces [45]. The diameters of the semicircles for the $CoWO_4$/RGO electrodes are generally smaller than those of the $CoWO_4$ electrode, and $CoWO_4$/RGO_5 has the smallest diameter, indicating lower interface resistance. This result validates that the $CoWO_4$/RGO composites with 1D-nanocube/2D-sheet heterostructure are beneficial to enhance the penetration of electrolyte and reduce charge-transfer resistance at the electrode/electrolyte interface.

The above results reveal that incorporating $CoWO_4$ with RGO could highly enhance the electrochemical properties $CoWO_4$ when it was used as an anode in LIBs.

Conclusion

In summary, a facile and green preparation approach for $CoWO_4$/RGO composites was developed based on the hydrothermal process without any additional reducing or dispersing agents. The as-prepared composites showed outstanding performance as anodes of LIBs with respect to capacity, rate capability, and cycling stability. The $CoWO_4$/RGO electrode exhibited initial charge-discharge capacities of 853 and 1441 mAh g^{-1} with an initial coulombic efficiency of 59.3%. A specific reversible capacity of ~ 530 mAh g^{-1} after 50 cycles at the specific current of 0.1 A g^{-1} was still obtained. The $CoWO_4$/RGO also displayed better capacity retention and exceptional high rate performance and cyclic stability as compared with $CoWO_4$. The excellent cycling performance can be ascribed to the synergistic effect between RGO and $CoWO_4$, which can enhance the electrical conductivity, provide a high contact area between the electrode and the electrolyte, shorten the transport pathway for both electrons and ions, and restrain volume expansion during the prolonged cycling. A combination of a facile synthesis, low cost, and excellent electrochemical performance enables $CoWO_4$/RGO to act as an alternative anode for LIBs with a high application potential.

Funding information The authors received financial support from the National Science Foundation (51573126).

References

1. Kang S, Li YY, Wu MM, Cai M, Shen PK (2014) Synthesis of hierarchically flower-like $FeWO_4$ as high performance anode materials for Li-ion batteries by a simple hydrothermal process. Int J Hydrog Energy 39(28):16081–16087
2. Hu ZL, Liu HD (2015) Three-dimensional CuO microflowers as anode materials for Li-ion batteries. Ceram Int 41(6):8257–8260
3. Wang RH, Xu CH, Du M, Sun J, Gao L, Zhang P, Yao HL, Lin CC (2014) Solvothermal-induced self-assembly of Fe_2O_3/GS aerogels for high Li-Storage and excellent stability. Small 10(11):2260–2269
4. Xing LL, Deng P, He B, Nie YX, Wu XL, Yuan S, Cui CX, Xue XY (2014) Assembly of $FeWO_4$-SnO_2 core-shell nanorods and their high reversible capacity as lithium-ion battery anodes. Electrochim Acta 118:45–50
5. Poizot P, Laruelle S, Grugeon S, Dupont L, Tarascon JM (2000) Nano-sized transition-metal oxides as negative-electrode materials for lithium-ion batteries. Nature 407(6803):496–499
6. Zhang LS, Wang ZH, Wang LZ, Xing Y, Li XF, Zhang Y (2014) Electrochemical performance of $ZnWO_4$/CNTs composite as anode materials for lithium-ion battery. Appl Surf Sci 305:179–185
7. Chai XH, Shi CS, Liu EZ, Li JJ, Zhao NQ, He CN (2015) Carbon-coated Fe_2O_3 nanocrystals with enhanced lithium storage capability. Appl Surf Sci 347:178–185
8. Lübke M, Makwana NM, Gruar R, Tighe C, Brett D, Shearing P, Liu ZL, Darr JA (2015) High capacity nanocomposite Fe_3O_4/Fe anodes for Li-ion batteries. J Power Sources 291:102–107
9. Chen MH, Xia XH, Yin JH, Chen QG (2015) Construction of Co_3O_4 nanotubes as high-performance anode material for lithium ion batteries. Electrochim Acta 160:15–21
10. Reddy MV, Prithvi G, Loh KP, Chowdari BVR (2014) Li storage and impedance spectroscopy studies on Co_3O_4, CoO, and CoN for Li-ion batteries. ACS Appl Mater Interfaces 6:680−690
11. Zhang JF, Pan JG, Shao LY, Shu J, Zhou MJ, Pan JG (2014) Micro-sized cadmium tungstate as a high-performance anode material for lithium-ion batteries. J Alloys Compd 614:249–252
12. Pullar RC, Farrah S, McN N (2007) $MgWO_4$, $ZnWO_4$, $NiWO_4$ and $CoWO_4$ microwave dielectric ceramics. Alford J Eur Ceram Soc 27(2-3):1059–1063
13. García-Pérez UM, Cruz AM, Peralc J (2012) Transition metal tungstates synthesized by co-precipitation method: basic photocatalytic properties. Electrochim Acta 81:227–232
14. Ungelenk J, Speldrich M, Dronskowski R, Feldmanna C (2014) Polyol-mediated low-temperature synthesis of crystalline tungstate nanoparticles MWO_4 (M¼Mn, Fe, Co, Ni, Cu, Zn). Solid State Sci 31:62–69
15. Ling C, Zhou LQ, Jia HF (2014) First-principles study of crystalline $CoWO_4$ as oxygen evolution reaction catalyst. RSC Adv 4(47): 24692–24697
16. Castillo TR, JS G'r, Ortiz AL, VC M'n (2013) Global kinetic evaluation during the reduction of $CoWO_4$ with methane for the production of hydrogen. Int J Hydrog Energy 38(28):12519–12526
17. Yu P, Wang L, Liu X, Fu HG, Yu HT (2017) CoWO4 nanopaticles wrapped by RGO as high capacity anode material for lithium ion batteries. Rare Metals 36(5):411–417

18. Greenn SV, Granqvist CG, Niklasson GA (2014) Structure and optical properties of electrochromic tungsten-containing nickel oxidefilms. Sol Energy Mater Sol Cells 126:248–259
19. Chen G, Rodriguez R, Fei L, Xu Y, Deng SG, Smirnov S, Luo HM (2014) A facile hydrothermal route to Fe_2O_3 with conductive additives as composite anode for lithium ion batteries. J Power Sources 259:227–232
20. Fu M, Jiao QZ, Zhao Y (2014) One-step vapor diffusion synthesis of uniform CdS quantum dots/reduced graphene oxide composites as efficientvisible-light photocatalyst. RSC Adv 4(44):23242–23250
21. Zhang M, Yan FL, Tang X, Li QH, Wang TH, Cao GZ (2014) Flexible CoO-graphene-carbon nanofiber mats as binder-free anodes for lithium-ion batteries with superior rate capacity and cyclic stability. J Mater Chem A 2(16):5890–5897
22. Sun CW, Li F, Ma C, Wang Y, Ren YL, Yang W, Ma ZH, Li JQ, Chen YJ, Kim Y, Chen LQ (2014) Graphene-Co_3O_4 nanocomposite as an efficient bifunctional catalyst for lithium-air batteries. J Mater Chem A 2(20):7188–7196
23. Guo R, Yue WB, An YM, Ren Y, Yan X (2014) Graphene-encapsulated porous carbon-ZnO composites as highperformance anode materials for Li-ion batteries. Electrochim Acta 135:161–167
24. Ren JG, Wang CD, Wu QH, Liu X, Yang Y, Fang L, Zhang WJ (2014) A silicon nanowire–reduced graphene oxide composite as a high-performance lithium ion battery anode material. Nano 6: 3353–3360
25. Li SM, Wang B, Liu JH, Yu M (2014) In situ one-step synthesis of $CoFe_2O_4$/graphene nanocomposites as high-performance anode for lithium-ion batteries. Electrochim Acta 129:33–39
26. Xu XD, Jeong S, Rout CS, Oh P, Ko M, Kim H, Kim MG, Cao RG, Cho HSJ (2014) Lithium reaction mechanism and high rate capability of VS_4-graphene nanocomposite for lithium battery anode material. J Mater Chem A 2(28):10847–10853
27. Li ZT, Wu GL, Liu D, Wu WT, Jiang B, Zheng JT, Li YP, Li JH, Wu MB (2014) Graphene enhanced carbon-coated tin dioxide nanoparticles for lithium-ion secondary battery. J Mater Chem A 2(20): 7471–7477
28. Zhen L, Wang WS, Xu CY, Shao WZ, Qin LC (2008) A facile hydrothermal route to the large-scale synthesis of $CoWO_4$ nanorods. Mater Lett 62(10-11):1740–1742
29. Thongtema S, Wannapop S, Thongtem T (2009) Characterization of $CoWO_4$ nano-particles produced using the spray pyrolysis. Ceram Int 35(5):2087–2091
30. Li LZ, Chen MX, Huang GB, Yang N, Zhang L, Wang H, Liu Y, Wang W, Gao JP (2014) A green method to prepare Pd-Ag nanoparticles supported on reduced graphene oxide and their electrochemical catalysis of methanol and ethanol oxidation. J Power Sources 263:13–21
31. Na HY, Zhang L, Qiu HX, Wu T, Chen MX, Yang N, Li LZ, Xing FB, Gao JP (2015) A two step method to synthesize palladiumecopper nanoparticles on reduced graphene oxide and their extremely high electrocatalytic activity for the electrooxidation of methanol and ethanol. J Power Sources 288:160–167
32. Jia HF, Stark J, Zhou LQ, Ling C, Sekito T, Markin Z (2012) Different catalytic behavior of amorphous and crystalline cobalt tungstate for electrochemical water oxidation. RSC Adv 2(29): 10874–10881
33. Zhang CL, Guo DL, Hu CG, Chen YX, Hong L, Zhang HL, Wang X (2013) Large-scale synthesis and photoluminescence of cobalt tungstate nanowires. Phys Rev B 87(3):35416
34. Li FH, Guo YQ, Liu Y, Qiu HX, Sun XY, Wang W, Liu Y, Gao JP (2013) Fabrication of Pt–Cu/RGO hybrids and their electrochemical performance for the oxidation of methanol and formic acid in acid media. Carbon 64:11–19
35. Zhang X, Liu HH, Petnikota S, Ramakrishna S, Fan HJ (2014) Electrospun Fe_2O_3–carbon composite nanofibers as durable anode materials for lithium ion batteries. J Mater Chem A 2(28):10835–10841
36. Shi NX, Xiong SL, Wu FF, Bai J, Chu YT, Mao HZ, Feng JK, Xi BJ (2017) Hydrothermal synthesis of $ZnWO_4$ hierarchical hexangular microstars for enhanced lithium-storage properties. Eur J Inorg Chem 2017(3):734–740
37. Shim HW, Cho IS, Hong KS, Lim AH, Kim DW (2011) Wolframite-type $ZnWO_4$ nanorods as new anodes for Li-ion batteries. J Phys Chem C 115(32):16228–16233
38. Li BS, Feng JK, Qian YT, Xiong SL (2015) Mesoporous quasi-single-crystalline $NiCo_2O_4$ superlattice nanoribbons with optimizable lithium storage properties. J Mater Chem A 3(19): 10336–10344
39. Ye Y, Wu P, Zhang X, Zhou T, Tang YW, Zho YM, Lu TH (2014) Facile synthesis of graphene supported $FeSn_2$ nanocrystals with enhanced li-storage capability. RSC Adv 4:17401C17404
40. Qiu BC, Xing MY, Zhang JL (2014) Mesoporous TiO_2 nanocrystals grown in situ on graphene aerogels for high photocatalysis and lithium-ion batteries. J Am Chem Soc 136(16):5852–5855
41. Geng H, Kong SF, Wang Y (2014) NiS nanorods-assembled nanoflower grown on graphene: morphology evolution and li-ion storage application. J Mater Chem A 2(36):15152–15158
42. Hong W, Li LZ, Xue RN, Xu XY, Wang H, Zhou JK, Zhao HL, Song YH, Liu Y, Gao JP (2017) One-pot hydrothermal synthesis of zinc ferrite/reduced graphene oxide as an efficient electrocatalyst for oxygen reduction reaction. J Colloid Interface Sci 485:175–182
43. Zhang GQ, Wu HB, Song T, Paik U, Wen X (2014) TiO_2 hollow spheres composed of highly crystalline nanocrystals exhibit superior lithium storage properties. Angew Chem Int Ed 53(46):12590–12593
44. Yu YJ, Yue C, Sun SB, Lin W, Su H, Xu BB, Li JT, Wu ST, Li J, Kang JY (2014) The effects of different core−shell structures on the electrochemical performances of Si−Ge nanorod arrays as anodes for micro-lithium ion batteries. ACS Appl Mater Interfaces 6(8): 5884–5890
45. Wang N, Liu QL, Kang DM, Gu JJ, Zhang W, Zhang D (2016) Facile self-cross-linking synthesis of 3D nanoporous Co_3O_4/carbon hybrid electrode materials for supercapacitors. ACS Appl Mater Interfaces 8:16035–16044